applied sciences

MDPI

Article

Development of Virtual Sensor Based on LSTM-Autoencoder to Detect Faults in Supply Chilled Water Temperature Sensor

San Jin [1], Ahmin Jang [1], Donghoon Lee [2], Sungjin Kim [2], Minjae Shin [3] and Sung Lok Do [1,*]

[1] Department of Building and Plant Engineering, Hanbat National University, Daejeon 34158, Republic of Korea; jinsan9708@naver.com (S.J.); jam2990@naver.com (A.J.)
[2] Department of Architectural Engineering, Hanbat National University, Daejeon 34158, Republic of Korea; donghoon@hanbat.ac.kr (D.L.); sungjinkim@hanbat.ac.kr (S.K.)
[3] Division of Architecture and Architectural Engineering, College of Engineering Sciences, Hanyang University, Ansan 15588, Republic of Korea; mshin@hanyang.ac.kr
* Correspondence: sunglokdo@hanbat.ac.kr

Abstract: Supply chilled water temperature (SCWT) is an important variable for the efficient and stable operation of heating, ventilation, and air conditioning (HVAC) systems. A precisely measured value ensured by the continuous reliability of the temperature sensor is essential for optimal control of an HVAC system because temperature sensor faults can affect the chiller operation and waste energy. Therefore, temperature sensor fault-detection strategies are imperative for maintaining a comfortable indoor thermal environment and ensuring the efficient and stable operation of HVAC systems. This study proposes a fault-detection method for an SCWT sensor using a virtual sensor based on a long short-term memory-autoencoder. The fault-detection performance is evaluated considering a case study under various sensor fault scenarios to evaluate changes in indoor thermal comfort and energy consumption after correcting sensor faults detected by the virtual sensor. The results verify excellent fault-detection performance in various fault scenarios (F-1 scores ranging from 0.9350 to 1.000). After correcting the SCWT fault, indoor thermal comfort is steadily maintained without additional energy consumption (indoor set-point temperature unmet hour reduced by a maximum of 105.7 hours, and energy consumption decreased by up to 1.8%).

Keywords: supply chilled water temperature sensor; sensor fault; indoor thermal comfort; energy consumption; fault detection; virtual sensor

Citation: Jin, S.; Jang, A.; Lee, D.; Kim, S.; Shin, M.; Do, S.L. Development of Virtual Sensor Based on LSTM-Autoencoder to Detect Faults in Supply Chilled Water Temperature Sensor. *Appl. Sci.* **2024**, *14*, 1113. https://doi.org/10.3390/app14031113

Academic Editor: Giuseppe Lacidogna

Received: 20 November 2023
Revised: 8 January 2024
Accepted: 13 January 2024
Published: 29 January 2024

1. Introduction

Heating and cooling energy consumption accounts for approximately 56.5% of the total energy consumption in commercial buildings in South Korea [1]. Furthermore, the global warming has resulted in a decrease in heating degree days and a gradual increase in cooling degree days. Consequently, the demand for cooling energy in commercial buildings is expected to gradually rise [2]. Therefore, it is essential to operate chillers in an energy-efficient manner because they account for the largest proportion of energy consumption in a cooling system. The energy consumption of a chiller is influenced by the return water temperature and supply chilled water temperature (SCWT). The return water temperature varies based on the mixed air temperature encountered by the cooling coil, which is influenced by outdoor and indoor loads. Thus, return water temperature has a limited direct correlation with the energy-efficient operation of a chiller. Conversely, a chiller assesses the satisfaction of a set point for the SCWT by measuring the actual SCWT. Consequently, the supply water temperature has a substantial impact on a chiller's efficiency because it determines the necessary work of the compressor. Accurate measurement of the SCWT is essential for achieving energy-efficient operation of a chiller. However, SCWT sensors are exposed to environmental factors such as temperature, humidity, and vibrations that can lead to sensor faults. Faults in the SCWT sensor not only reduce the chiller efficiency but

also potentially cause thermal discomfort for occupants [3]. This arises solely from sensor faults and not from faults in the chiller. Therefore, it is crucial to detect sensor faults to maintain the accuracy of SCWT sensors.

Detection methods for faults in physical sensors within heating, ventilation, and air conditioning (HVAC) systems, including the SCWT sensor, are categorized as rule-based modeling or data-driven methods [4]. The rule-based model detects sensor faults by explicitly assessing the conformity of the input data to predefined algorithms [5–8]. Data-driven methods employ machine learning or artificial intelligence techniques to detect faults, and models are trained on fault patterns. Rule-based modeling is based on simple physics, with the advantage of being easy to understand. In addition, the relationship between the input and output data is straightforward. However, this model has limited flexibility that leads to lower detection rates for complex or novel data and fault patterns. This model also has disadvantages, such as high model update costs and challenges in automation. The data-driven method does not explain the internal workings of the model but has the advantages of abundant data availability and ease of model development. The data-driven method is more convenient for sensor fault detection than rule-based modeling, and research on fault-detection technology using data-driven methods is being conducted.

Wang et al. developed a sensor fault-detection and diagnostic method based on the principal component analysis (PCA) model [9]. This PCA model learned the correlation between the sensors installed within the cooling system and evaluated the square prediction error of the data to detect sensor faults. This model demonstrated excellent fault-detection performance through simulation tests, assuming four types of sensor faults.

Another study argued that it was necessary to address sensor faults before detecting other faults in the overall HVAC system to ensure reliable fault detection [10]. Accordingly, a sensor fault-detection strategy based on PCA was introduced that exhibited the capability of detecting various sensor faults, achieving detection rates of 82% to 100%.

Yan et al. developed a Boltzmann-machine-based method for detecting faults in sensors within HVAC systems [11]. This approach involved assessing the occurrence of sensor faults by exchanging information between sensors. The fault-detection performance of this model attained F-1 scores ranging from 0.92 to 1.00 across various types of sensor faults.

Lee et al. proposed a fault-detection method based on a generalized regression neural network (GRNN) model to detect system and sensor faults within an air handling unit (AHU) [12]. The GRNN model compared newly acquired and previously learned data to generate residuals. Faults were detected based on whether the residuals exceeded a specified threshold. This study categorized various potential fault types within the AHU and simulated cases to evaluate the fault-detection performance of the GRNN model. Through case-specific simulations, the GRNN fault-detection model was deemed beneficial for real-time fault detection.

Du et al. proposed a dual-coupled artificial neural network (ANN)-based fault-detection strategy to detect sensor faults in the supply air temperature control loop of HVAC systems [13]. Primary and auxiliary ANNs were developed through control and variable correlation analyses by combining the two ANNs, and the performance was evaluated in the cases of fixed offset, drift offset, and complete sensor failure. This fault-detection method exhibited false alarm rates (the ratio of normal conditions incorrectly identified as faults) ranging from 0.6% to 7.5% and missed detection rates (the ratio of faults incorrectly identified as normal) ranging from 0% to 8.3% across all fault occurrence scenarios.

The research related to sensor fault detection within HVAC systems using the data-driven method are summarized in Table 1.

Table 1. Literature review of sensor fault detection.

Ref.	Year	Method	Sensor Fault Type	Quantitative Result
[9]	2004	PCA	Fixed bias Drifting Precision degradation Complete failure	Detection ratio: almost 100%
[10]	2010	PCA	Fixed bias	Detection ratio: 96.4–100%
[11]	2022	Boltzmann-machine	Fixed bias	F-1 score: 0.92–1.00
[12]	2004	GRNN	Fixed bias	Fault classification: O
[13]	2014	Combined ANN	Fixed bias	False alarm ratio: 0.6–7.5% Missing alarm ratio: 0–8.3%

The following issues from the literature review must be considered:

- A chiller operates continuously in response to outdoor and indoor environments, and it is difficult to distinguish between sensor faults based on the acquired data. Furthermore, situations in which a chiller operates under sensor faults are uncommon, and it is difficult to obtain fault data. Accordingly, the imbalance of the acquired data adversely affects the performance of the fault-detection models.
- There has been a lack of research on detecting faults in SCWT sensors and evaluating indoor thermal comfort and energy consumption by correcting sensor faults.

Therefore, this study developed a virtual sensor for detecting faults in the SCWT sensor. Subsequently, a case study was conducted using EnergyPlus to simulate scenarios of SCWT sensor faults. This approach facilitated the evaluation of the fault-detection performance and effects resulting from sensor fault correction. Detailed information about the methodology of this study and development of the virtual sensor is presented in Sections 2 and 3, respectively.

2. Methodology

The aim of this study was to develop a virtual sensor for detecting faults in a SCWT sensor and evaluate its fault-detection performance and correction effects. Accordingly, this study was conducted in five steps, as shown in Figure 1.

The first step involved developing a simulation model. For the case study, an office building, cooling system, and faults in the SCWT sensor were modeled using a building energy simulation tool, EnergyPlus. The second step involved the development of a virtual sensor based on a long short-term memory (LSTM)-autoencoder. Detailed information about the LSTM-Autoencoder is presented in Section 3. The third step involved the classification of the simulation cases according to the fault type. Fault scenarios were assumed and categorized into simulation cases, and datasets were created based on the simulation results for each case. Various types of fault data were input into the virtual sensor to evaluate the fault-detection performance and correction effect of the virtual sensor. The fourth step involved evaluating the fault-detection performance of the virtual sensor. The results of fault detection using the virtual sensor were analyzed, and the fault-detection performance was evaluated using four performance metrics. Finally, the fifth step involved evaluating the fault correction effect of the virtual sensor. This step constituted evaluating the impact on the indoor set-point temperature unmet hours, energy consumption resulting from the correction of SCWT sensor faults by the virtual sensor, sensor calibration, and replacement.

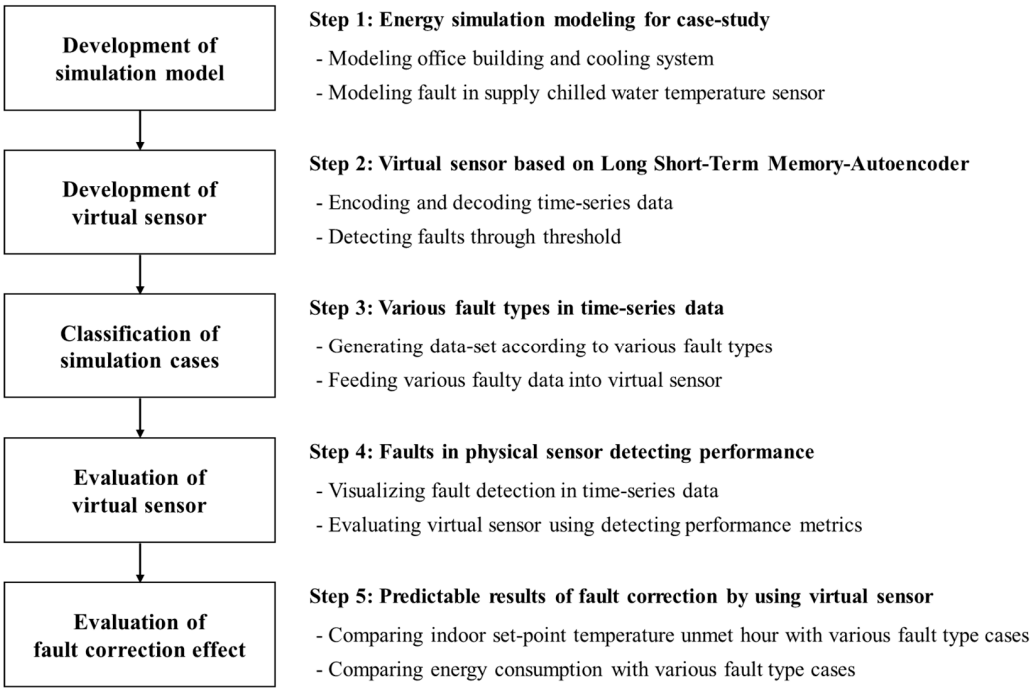

Figure 1. Overall research process.

3. Development of Virtual Sensor

3.1. LSTM-Autoencoder

3.1.1. LSTM

LSTM is a type of recurrent neural network (RNN). The gradient vanishing problem of traditional RNNs in long-term memory is improved through the structure (input, forget, and output gates) [14,15]. Accordingly, various studies have been conducted using LSTM in the HVAC field, which mainly deal with variables (such as energy consumption and load) influenced by data from previous time steps [16–19]. The LSTM structure is shown in Figure 2.

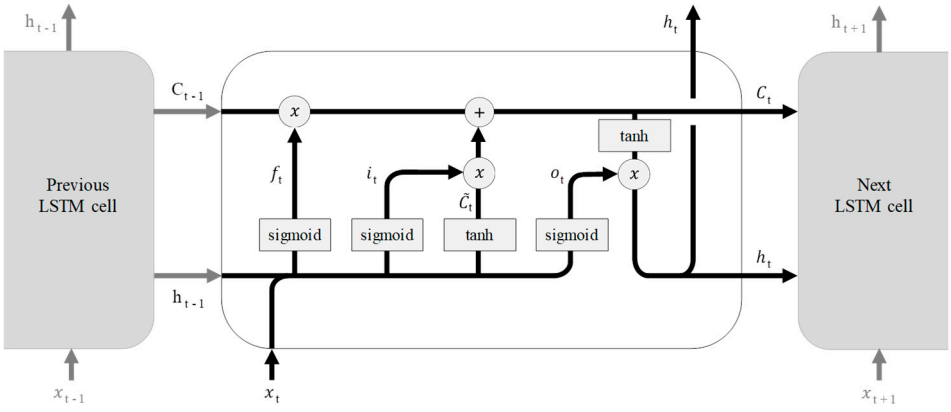

Figure 2. LSTM structure.

The working principle of LSTM is as follows. In the first step, the time-series data are input in vector form, and the forget gate determines the extent to which the previous time-step information should be forgotten. The degree of forgetting is determined by passing the current time-step information and previous time-step hidden layer value through a sigmoid function that outputs a value between 0 and 1. The degree of forgetting increases as the

value of the forget gate approaches zero. Conversely, the degree of forgetting decreases as the value approaches 1. The forget gate is calculated as follows:

$$f_t = \sigma\Big(W_{xf}x_t + W_{hf}h_{t-1} + b_f\Big), \tag{1}$$

where f_t denotes the forget gate, σ denotes the sigmoid function, W_{xf} denotes the weight used in the forget gate, x_t denotes the current time-step information, h_{t-1} denotes the value of the previous time-step hidden layer, W_{hf} denotes the weight used for h_{t-1} in the forget gate, and b_f denotes the bias of the forget gate.

In the second step, the input gate determines the extent to which the current time-step information should be remembered. To achieve this, the current time-step information and value of the previous time-step hidden layer are passed through a sigmoid function to output the input gate. Additionally, the current time-step information and value of the previous time-step hidden layer are passed through a tanh function to output the memory cell state. The input gate and state of the memory cell are respectively calculated as follows:

$$i_t = \sigma(W_{xi}x_t + W_{hi}h_{t-1} + b_i), \tag{2}$$

$$\widetilde{C}_t = \tanh(W_{xc}x_t + W_{hc}h_{t-1} + b_c), \tag{3}$$

where i_t denotes the input gate, W_{xi} denotes the weight used in the input gate, W_{hi} denotes the weight used for h_{t-1} in the input gate, b_i denotes the bias of the input gate, $\widetilde{C}_t$ denotes the state of the memory cell, tanh denotes the hyperbolic tangent function, W_{xc} denotes the weight used in the memory cell state, W_{hc} denotes the weight used for h_{t-1} in the memory cell state, and b_c denotes the bias of the memory cell state.

In the third step, the memory cell is updated at the current time step. The memory cell at the current time step is calculated using the previously calculated forget gate, input gate, and memory cell state and then passed to the memory cell at the next time step. The updated state of the memory cell is calculated as follows:

$$C_t = f_t * C_{t-1} + i_t\widetilde{C}_t, \tag{4}$$

where C_t denotes the updated state of the memory cell at the current time step and C_{t-1} denotes the memory cell state passed from the previous time step.

In the fourth step, the output gate determines the extent of the output information from the current time-step hidden-layer values. The output degree of the hidden layer values is determined by passing the current time-step information and value of the previous time-step hidden layer through a sigmoid function to output the output gate. Subsequently, this output is multiplied by the memory cell at the current time step and passed through a tanh function. At this time, the output information is sent to the hidden layer or LSTM cell at the next time step. The output gate and final output information are respectively expressed as follows:

$$o_t = \sigma(W_{xo}x_t + W_{ho}h_{t-1} + b_o), \tag{5}$$

$$h_t = o_t * \tanh(C_t), \tag{6}$$

where o_t denotes the output gate, W_{xo} denotes the weight used for x_t in the output gate, W_{ho} denotes the weight used for h_{t-1} in the output gate, b_o denotes the bias of the output gate, and h_t denotes the final output information being sent from the current time step to the next time step.

3.1.2. Autoencoder

An autoencoder is an RNN used for unsupervised learning that consists of a basic structure with input, hidden, and output layers. The hidden layer is divided into an encoder, latent vector, and decoder, as illustrated in Figure 3. The autoencoder has fewer neurons in

the hidden layer than in the input and output layers owing to this structure, resulting in a bottleneck shape in which the number of neurons in the input and output layers is equal. The working principle of the autoencoder is as follows. The encoder learns the unique characteristics of the input data as they are input into the autoencoder and then compresses them to extract the latent vector. The decoder reconstructs the compressed data to produce output data similar to the original input data (data before compression). However, the output data cannot be identical to the original input data owing to compression by the encoder and reconstruction by the decoder. As a result, there is a reconstruction error between the original input and output data. The autoencoder is trained to minimize the reconstruction error.

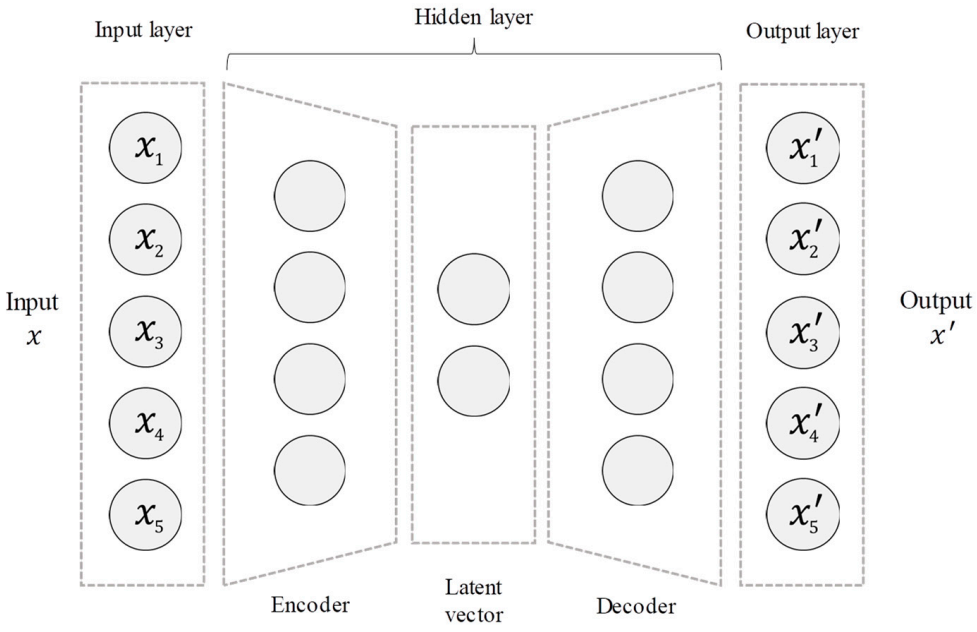

Figure 3. Generic structure of autoencoder.

3.2. Virtual Sensor for Fault Detecting in Physical Sensor

3.2.1. Virtual Sensor Based on LSTM-Autoencoder

The LSTM-autoencoder was used to develop the virtual sensor for fault detection in an SCWT sensor and consisted of an LSTM-based encoder and decoder. The process for detecting faults in a physical sensor using the virtual sensor proposed in this study is shown in Figure 4.

The first step is normal time-series data training (Figure 4a). The LSTM-autoencoder compresses the normal time-series data using the LSTM encoder and then reconstructs the data using the LSTM decoder. During this process, the LSTM-autoencoder learns only the characteristics of normal time-series data. The second step is the input of unlabeled time-series data (Figure 4b). Here, the LSTM-autoencoder outputs a high reconstruction error when the input data contains faults. The third step is sensor fault detection (Figure 4c). Here, the reconstruction error generated as faulty time-series data is used as input. The virtual sensor determines that the physical sensor is faulty if the reconstruction error exceeds the threshold value.

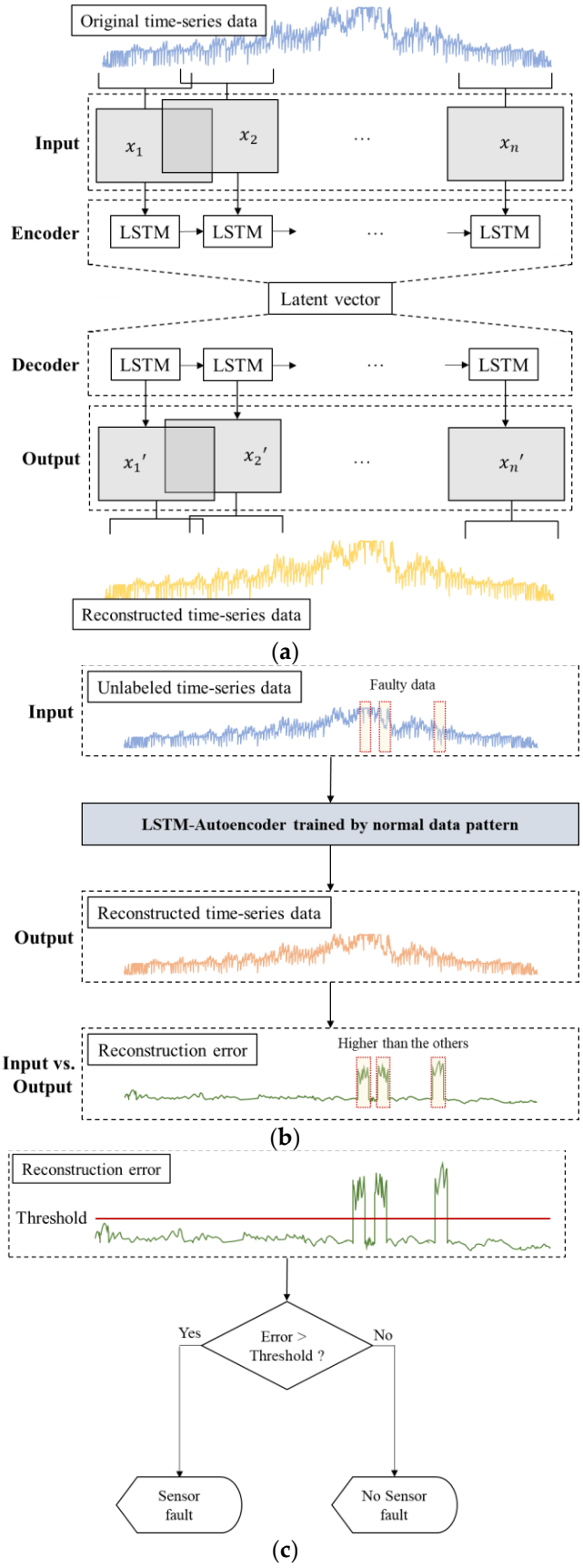

Figure 4. Fault detection using the proposed virtual sensor. (**a**) Step 1: normal time-series data training; (**b**) step 2: input of unlabeled time-series data; and (**c**) step 3: fault detection.

3.2.2. Virtual Sensor Modeling

A virtual sensor based on an LSTM-autoencoder was developed to detect faults in an SCWT sensor. The hyperparameters and input variables for the LSTM-autoencoder are listed in Table 2. The input variables for the virtual sensor training were obtained using EnergyPlus, as described in Section 4.

Table 2. Parameters of the LSTM-autoencoder.

Parameter			Value
Hyper parameters	Layers	LSTM encoder	140 70
		LSTM decoder	70 140
	Optimizer		Adam
	Activation function		ReLU
	Loss function		Mean squared error
	Batch size		32
	Epochs		100
Input parameters			Outdoor air temperature Chiller energy consumption SCWT

4. Case Study

A case study was conducted to evaluate the fault-detection performance and correction effect of the virtual sensor. To achieve this, a commercial building and faults in an SCWT sensor were modeled using EnergyPlus, and simulations were performed. The virtual sensor proposed in this study was trained using a dataset produced via simulations.

4.1. Simulation Modeling

4.1.1. Target Building and System

A single-story office building was modeled based on a medium-sized office-building model provided by the U.S. Department of Energy [20]. The weather data used for the simulation were sourced from the International Weather Files for Energy Calculation 2.0 for Daejeon, South Korea [21]. The thermal transmittance of the structure was set to satisfy the criteria for energy-saving design in central region 2 [22]. The cooling system applied to the building model was a variable air volume system consisting of a supply fan, cooling coil, circulation pump, water-cooled chiller, and cooling tower. The supply fan was modeled to variably control the supply air flow based on a partial load to meet the supply air set-point temperature. The circulation pump was modeled to variably control the supply chilled water flow based on the exit air temperature of the cooling coil. The chiller was modeled to variably control the chilled water flow to meet the chilled water set-point temperature. The set-point temperatures for the supply chilled water, supply air, and indoor air were 6.7 °C, 14 °C, and 26 °C, respectively. August was selected as the simulation period, which was the month with the highest annual average outdoor air temperature in Daejeon (Figure 5). The simulations were performed at 1-min intervals. The detailed input variables used for the simulation modeling are summarized in Table 3, and the building model envelope and cooling system schematics are shown in Figure 6.

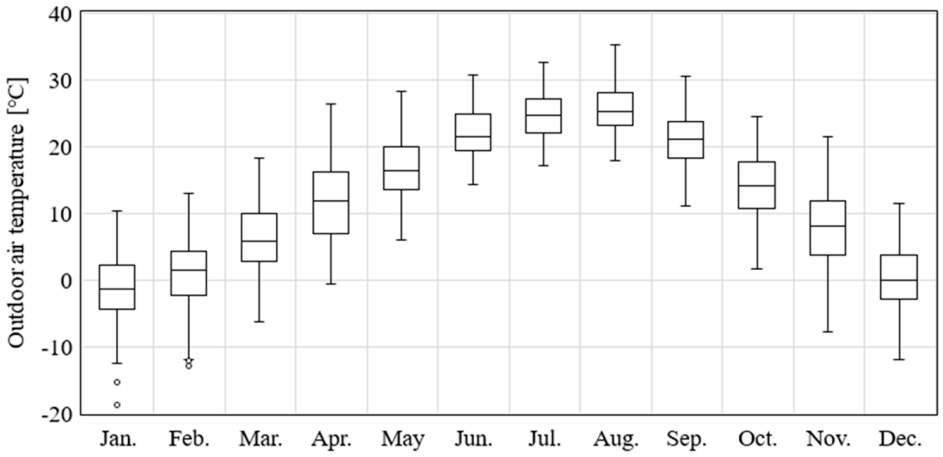

Figure 5. Monthly outdoor air temperature distribution in Daejeon, South Korea.

Table 3. Input parameters for simulation modeling.

Input Parameter			Value
Building	Zone	Location	Daejeon, South Korea
		Type	Office
		Zone volume	4800 m^3
		Indoor set-point temp.	26 °C
	U-values	Exterior wall	0.24 $W/m^2 \cdot K$
		Window	1.50 $W/m^2 \cdot K$
		Roof	0.15 $W/m^2 \cdot K$
		Floor	0.29 $W/m^2 \cdot K$
	Zone conditions	People	117.24 W/person
		Light	6.89 W/m^2
		Equipment	8.07 W/m^2
System	Capacity	Supply fan	2.7 m^3/s
		Circulation pump	0.003 m^3/s
		Chiller	70,000 W
Simulation setting		Run period	8/1 to 8/31
		Time step	1 min

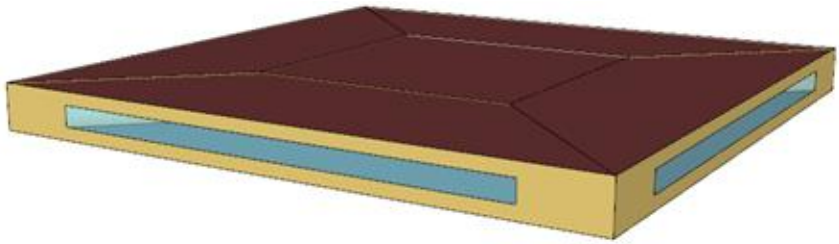

(**a**)

Figure 6. *Cont.*

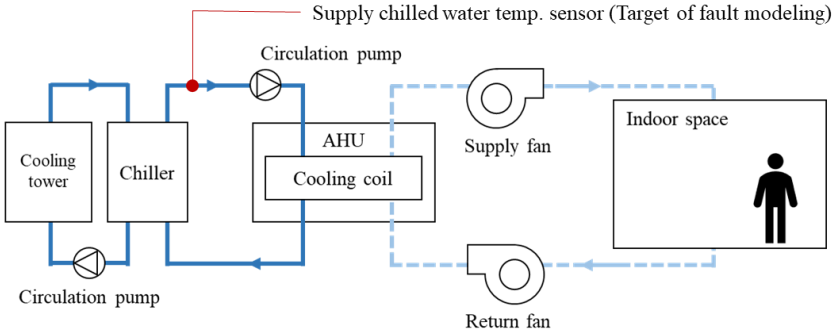

(**b**)

Figure 6. Schematics of the simulation model: (**a**) envelope of building; and (**b**) simplified cooling system.

4.1.2. SCWT Sensor Fault

EnergyPlus provides 16 fault models (such as coil fouling and various sensor faults) to simulate the impact of faults occurring in sensors, controllers, and equipment within HVAC systems. In this study, the TemperatureSensor:Offset:ChillerSupplyWater fault model was utilized because it focuses on faults in the SCWT sensor. This fault model allows the user to directly input the sensor fault schedules and offset values. The measured SCWT, supply chilled water flow rate, and cooling capacity of the chiller are calculated when this fault model is applied. The measured SCWT is expressed as follows:

$$T_{scw,f} = T_{scw,a} - \Delta T, \tag{7}$$

where $T_{scw,f}$ represents the SCWT measured by the faulty sensor (°C), $T_{scw,a}$ represents the actual SCWT (°C), and ΔT denotes the sensor fault offset (°C). The supply chilled water flow rate is expressed as follows:

$$Q_{scw,f} = \frac{q_{ch,a}}{\rho \cdot C_p \cdot \left(T_{rcw,f} - T_{scw,des}\right)}, \tag{8}$$

where $Q_{scw,f}$ represents the supply chilled water flow rate in the case of a faulty sensor (m^3/s), $q_{ch,a}$ represents the actual cooling capacity of the chiller (W), ρ represents the density of water (kg/m^3), C_p represents the specific heat of water (J/kg·K), $T_{rcw,f}$ represents the chiller return water temperature in the case of a faulty sensor (°C), and $T_{scw,des}$ denotes the supply chilled water set-point temperature (°C). The cooling capacity of the chiller is expressed as follows:

$$q_{ch,f} = \rho \cdot Q_{scw,f} \cdot C_p \cdot \left(T_{rcw,f} - T_{scw,f}\right), \tag{9}$$

where $q_{ch,f}$ represents the cooling capacity of the chiller in the case of a faulty sensor (W).

4.2. Simulation Cases

Faults in time-series data are categorized into point, contextual, and collective anomalies [23]. The point anomaly is a temporary fault that deviates significantly from a normal time-series distribution. Contextual and collective anomalies are continuous faults that occur over a certain period within a normal time-series distribution. This study divided simulation cases according to the type of fault to simulate situations that may occur in the SCWT sensor, as listed in Table 4. In the point-offset cases (Cases A-1 and A-2), faults in the SCWT sensor occurred temporarily once a week for one hour. In the fixed-offset cases (Cases B-1 to B-4), faults with a constant offset occurred continuously for a certain period. In the random-offset case (Case C), faults with a random offset occurred for a certain period. In these cases, a random offset was created using the random number generation function in Excel. In the drift-offset cases (Cases D-1 and D-2), faults with offset gradually worsened over time. Fixed, random, and drift offsets occurred on 16 August and continued until

31 August. In the fixed- and random-offset cases, the offset at the previous time did not affect the offset at the current time. Therefore, fault detection was performed during the operating hours of the chiller, from 7 AM to 6 PM. However, fault detection was performed continuously in the drift-offset cases because the drift offset at the current time was affected by the offset at the previous time.

Table 4. Simulation cases with various fault types.

Fault Type	Offset Type	Simulation Case	Offset	Fault Occurrence Scenario
Point anomaly	Point	A-1	−3 °C	One hour each time, once a week
		A-2	3 °C	
Contextual & collective anomaly	Fixed	B-1	−3 °C	From 16 August to 31 August
		B-2	−1 °C	
		B-3	1 °C	
		B-4	3 °C	
	Random	C	−3 °C to 3 °C	
	Drift	D-1	−0.1 °C/h (max: −10 °C)	
		D-2	0.1 °C/h (max: 10 °C)	

4.3. Virtual Sensor Fault-Detection Performance Metrics

The fault-detection performance of the developed virtual sensor was evaluated using classification performance metrics: accuracy, precision, recall, and F-1 score. The fault-detection result values of the virtual sensor were divided into True Negative (TN), False Negative (FN), False Positive (FP), and True Positive (TP) (Figure 7). TN represents the cases in which the virtual sensor correctly identifies the actual normal data as normal. FN represents the cases in which the virtual sensor incorrectly identifies the actual normal data as a fault. FP represents cases in which the virtual sensor incorrectly identifies the actual faulty data as normal. TP represents the cases in which the virtual sensor correctly identifies the actual faulty data as a fault.

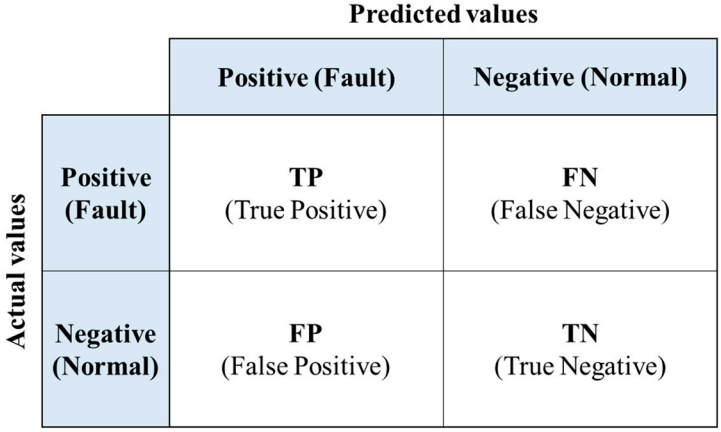

Figure 7. Confusion matrix according to fault-detection result values.

4.3.1. Accuracy

Accuracy indicates the proportion of data out of the total data in which the virtual sensor correctly identifies the actual normal data as normal and the actual faulty data as faults. The accuracy ranges from 0 to 1. The proportions of TN and TP increase as the accuracy increases. The accuracy is calculated using the following equation:

$$\text{Accuracy} = \frac{TN + TP}{TN + FP + FN + TP} \quad (10)$$

4.3.2. Precision

Precision indicates the proportion of all the faulty data that are identified by the virtual sensor as a fault. The precision has a value ranging from 0 to 1. The proportion of FP decreased as the precision increased. The precision is calculated using the following expression:

$$\text{Precision} = \frac{TP}{FP + TP} \tag{11}$$

4.3.3. Recall

Recall indicates the proportion of actual faulty data that the virtual sensor correctly identifies as a fault. Recall ranges from 0 to 1. The proportion of FN decreased as the recall increased. The recall is calculated using the following equation:

$$\text{Recall} = \frac{TP}{TP + FN} \tag{12}$$

4.3.4. F-1 Score

The F-1 score is used to prevent results in which precision or recall is biased because precision and recall have a trade-off relationship. The F-1 score is the harmonic mean value of precision and recall and has a value from 0 to 1. The fault-detection performance of the virtual sensor improved as the F-1 score increased. The F-1 score is calculated using the following expression:

$$\text{F-1 score} = 2 \times \frac{Precision \times Recall}{Precision + Recall} \tag{13}$$

5. Results

5.1. Virtual Sensor Fault-Detection Performance

The faults undetected by the virtual sensor are represented in the time-series data for the chiller energy consumption (represented as red dots in Figure 8). The fault-detection performance of the virtual sensor was evaluated using the four performance metrics listed in Table 5.

Table 5. Results of fault-detection performance of the virtual sensor.

Metrics	Simulation Case								
	A-1	**A-2**	**B-1**	**B-2**	**B-3**	**B-4**	**C**	**D-1**	**D-2**
Accuracy	1.0000	1.0000	0.9995	0.9998	0.9978	0.9980	0.9902	0.9510	0.8851
Precision	1.0000	1.0000	0.9985	0.9994	1.0000	1.0000	0.9993	0.9479	0.8778
Recall	1.0000	1.0000	1.0000	1.0000	0.9930	0.9937	0.9703	1.0000	1.0000
F-1 score	1.0000	1.0000	0.9992	0.9997	0.9965	0.9968	0.9846	0.9733	0.9350

All temporary faults that occurred in Cases A-1 and A-2 were detected to evaluate the fault-detection performance of the virtual sensor. The accuracy, precision, recall, and F-1 score values were 1.000. The virtual sensor showed excellent fault-detection performance for fixed offset (Cases B-1 to B-4) with all evaluation metrics ranging from 0.9930 to 1.000. The distribution of the performance metrics ranged from 0.9846 to 0.9993 for the random offset (Case C). However, it should be noted that the virtual sensor had difficulty detecting faults with small offset values among the random offsets. The distribution of all performance metrics ranged from 0.8851 to 1.000 in the drift offset (Cases D-1 and D-2). This indicated that the virtual sensor had difficulty detecting small offset values during the initial non-operating period of the chiller.

Overall, the proposed virtual sensor demonstrated excellent fault-detection performance in all cases. However, it exhibited difficulty in detecting faults with small offset values in Cases C, D-1, and D-2.

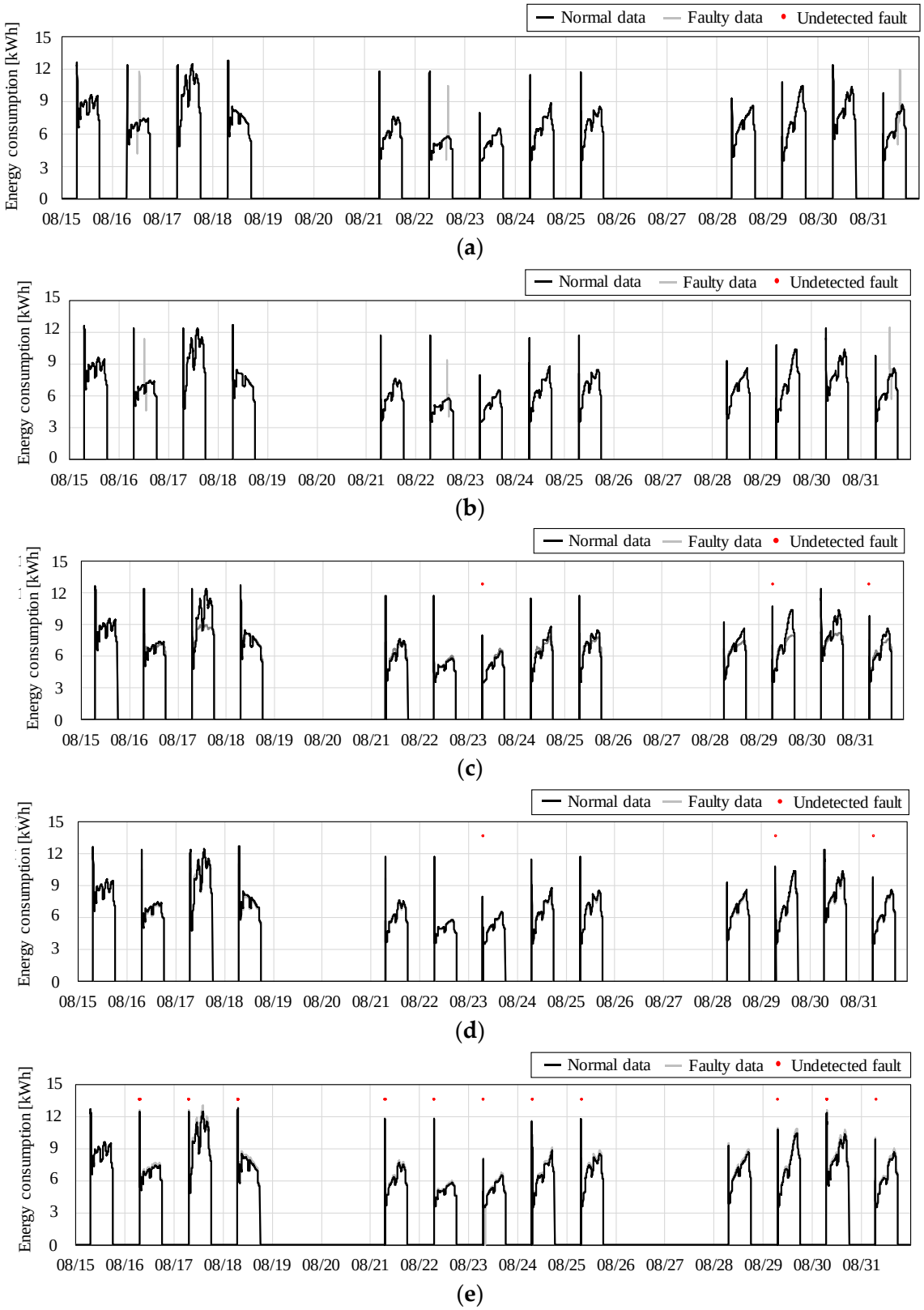

Figure 8. *Cont.*

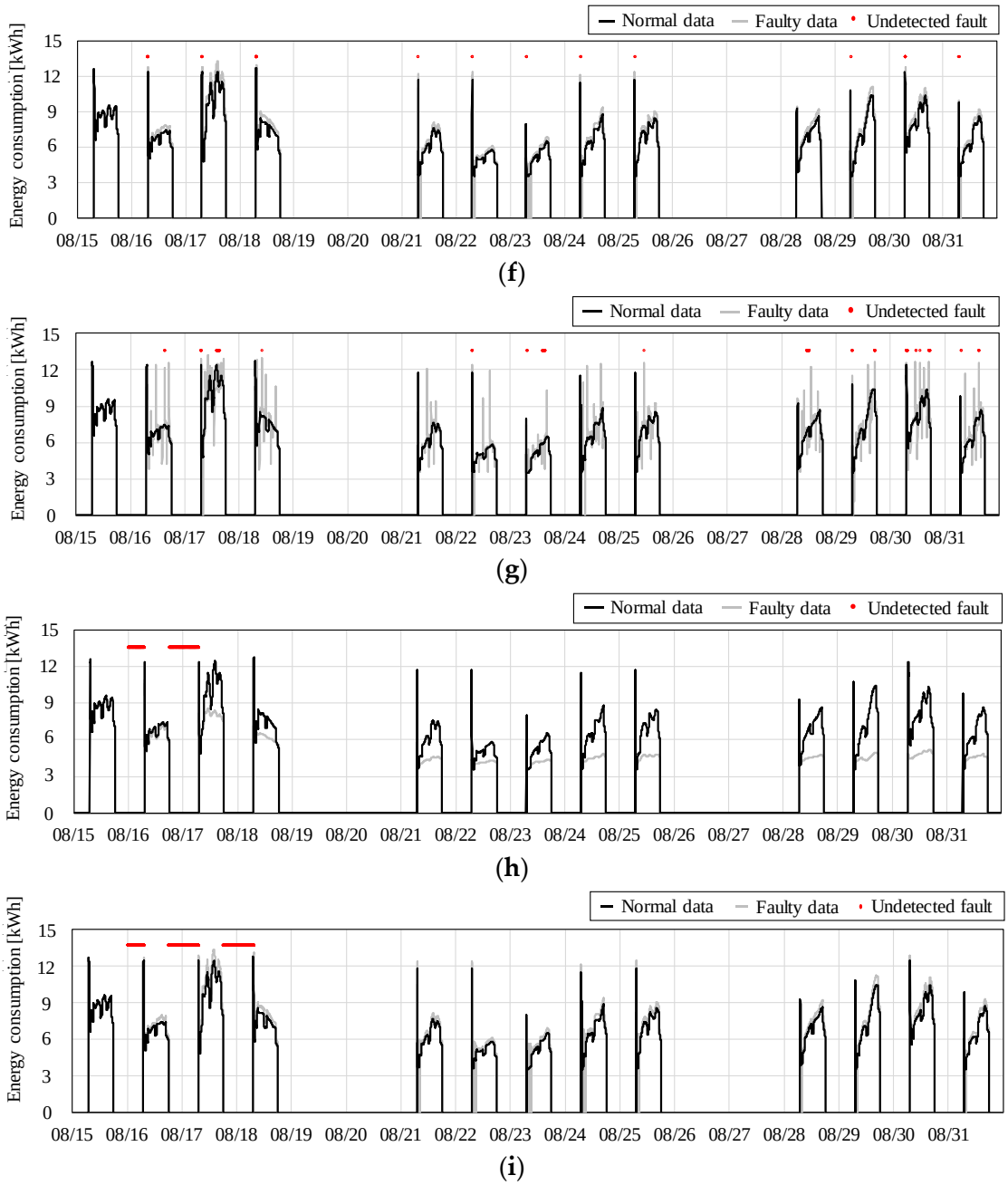

Figure 8. Results of fault detection with various time-series data: (**a**) Case A-1 (Point, offset: −3); (**b**) Case A-2 (Point, offset: 3); (**c**) Case B-1 (Fixed, offset: −3); (**d**) Case B-2 (Fixed, offset: −1); (**e**) Case B-3 (Fixed, offset: 1); (**f**) Case B-4 (Fixed, offset: −3); (**g**) Case C (Random, offset: −3 to 3); (**h**) Case D-1 (Drift, offset: −0.1 °C/h); and (**i**) Case D-2 (Drift, offset: 0.1 °C/h).

5.2. Virtual Sensor Fault-Correction Effect

The impact of detecting faults in the SCWT sensor was evaluated using a virtual sensor and by taking appropriate actions for correcting the sensor, such as sensor calibration or replacement. The evaluation focused on changes in indoor thermal comfort and energy consumption.

5.2.1. Indoor Set-Point Temperature Unmet Hours

The distribution of supply chilled water, air supply, indoor temperatures, and indoor set-point temperature unmet hours were analyzed to evaluate indoor thermal comfort

after correcting faults in the SCWT sensor. The distributions of monthly temperatures and indoor set-point temperature unmet hours with various fault types for supply chilled water, supply air, and indoor temperatures for each simulation case in August are shown in Figures 9 and 10, respectively.

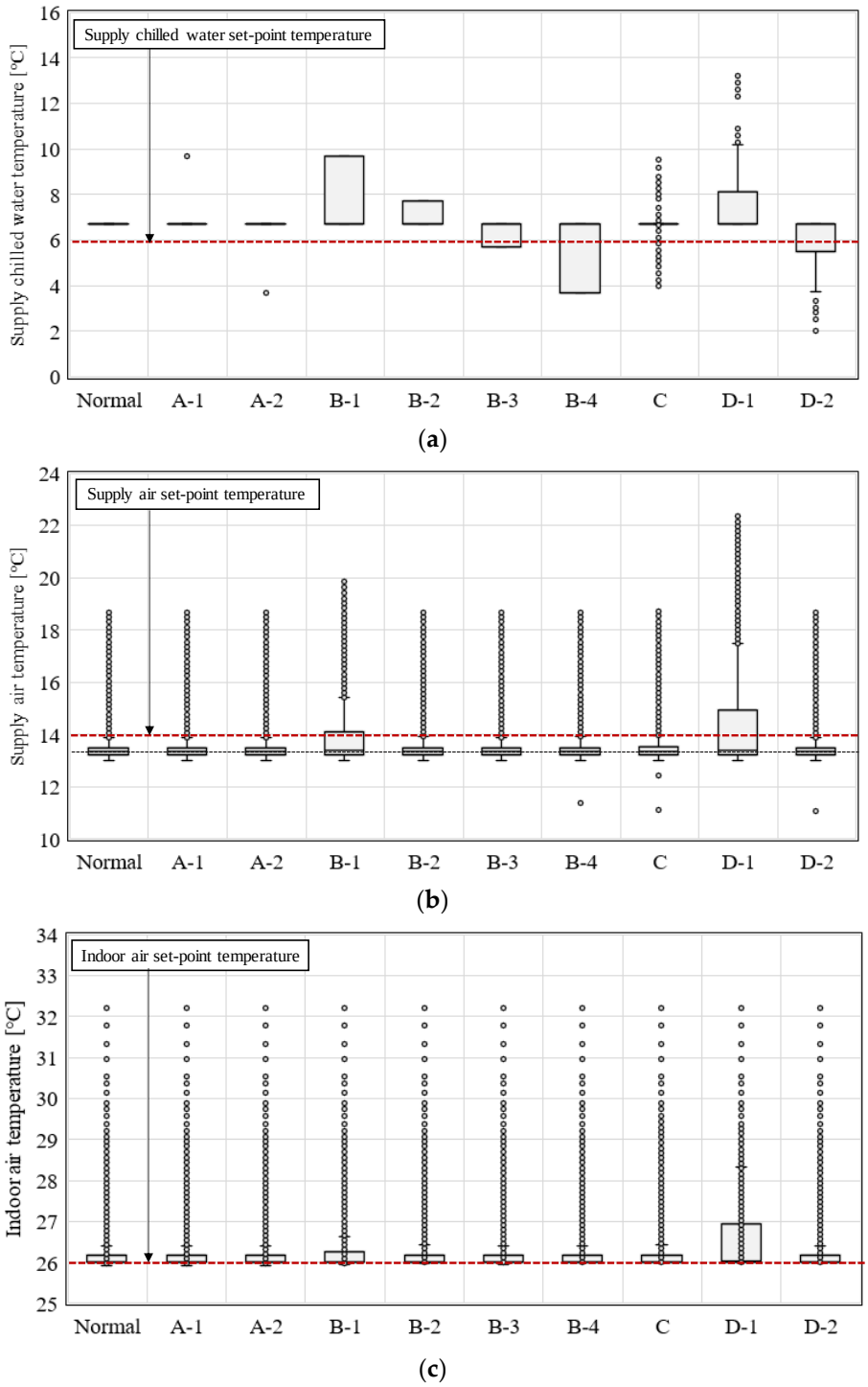

Figure 9. Distribution of monthly temperatures with various fault types: (**a**) supply chilled water; (**b**) supply air; and (**c**) indoor air temperature.

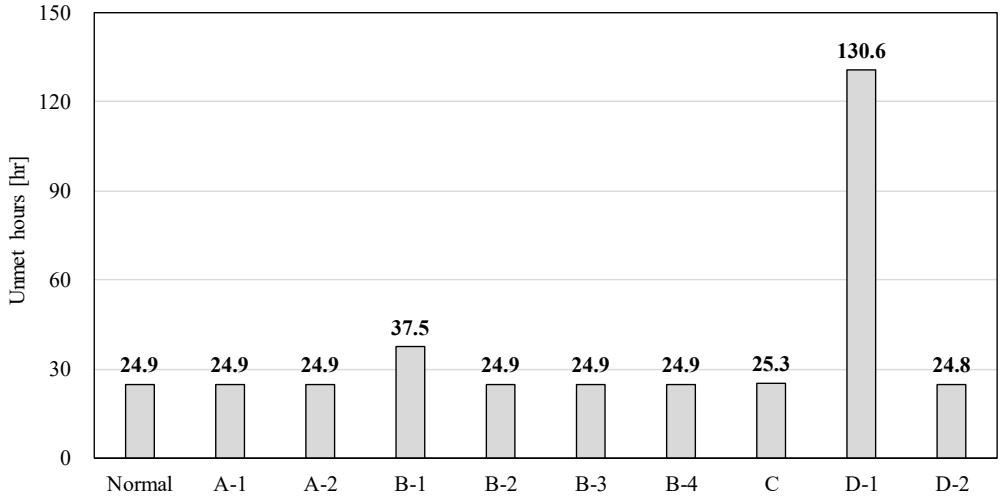

Figure 10. Indoor set-point temperature unmet hours with various fault types.

The impacts on indoor set-point temperature unmet hours and the distribution of supply chilled water, air supply, and indoor temperatures in Cases A-1 and A-2, where sensor faults occurred once a week for one hour, were comparable to those of the normal case (Figures 9 and 10). The impact on indoor thermal comfort varied depending on the frequency and offset of temporary fault occurrences because these cases assumed that the sensor faults only occurred for one hour per week. The fixed-offset cases (Cases B-1 and B-2) experienced faults with negative offsets in the SCWT sensor, resulting in increased distributions of the supply chilled water and supply air temperatures compared with those of the normal case (Figure 9a,b). Consequently, indoor temperature distribution increased, leading to approximately 12.6 and 0.1 h increases in indoor set-point temperature unmet hours (Figures 9c and 10). In contrast, Cases B-3 and B-4 had faults involving positive offsets in the SCWT sensor, which did not significantly impact the indoor set-point temperature during unmet hours or distributions of the chilled water supply, supply air, and indoor temperatures (Figures 9 and 10). Case C involved random sensor fault offsets that exhibited differences in the distribution of SCWT compared with that of the normal case. However, the supply air and indoor temperatures showed similar distributions (Figure 9). Consequently, indoor set-point temperature unmet hours increased by approximately 0.4 h (Figure 10). Among the drift offset cases, Case D-1 had a negative sensor fault offset, which resulted in a significant increase in the distributions of the supply chilled water, supply air, and indoor temperatures compared with those of the normal case (Figure 9). Consequently, the indoor set-point temperature unmet hours increased by 106.6 h (Figure 10). In contrast, Case D-2 had a positive sensor fault offset, which exhibited a lower distribution of SCWT compared with that of the normal case. However, the air supply and indoor temperature distributions as well as the indoor set-point temperature unmet hours remained similar (Figures 9 and 10).

The evaluation of indoor thermal comfort following the correction of faults in the SCWT sensor indicated that the impact of faults on indoor thermal comfort varied based on the fault occurrence frequency and offset. Faults with fixed or random offsets were likely to cause variations in their impact on thermal comfort. Additionally, faults with fixed offsets or those that changed gradually over time, especially with negative offsets, were found to adversely affect indoor thermal comfort, as evidenced by the increased indoor set-point temperature unmet hours (Table 6).

Table 6. Effects on indoor set-point temperature unmet hours for various fault types and offsets.

Offset	Negative Offset	Positive Offset
Point	Depended on offset value and frequency	
Fixed	Increase	Negligible
Random	Depended on offset value and frequency	
Drift	Increase	Decrease

5.2.2. Energy Consumption

Monthly chiller, circulation pump, and fan energy consumptions after the correction of faults in a SCWT sensor were evaluated for each simulation in August, as shown in Figure 11. The sensor faults had a limited impact on the energy consumption in Cases A-1 and A-2, where the frequency of sensor faults was low. Consequently, the circulation pump, fan, and chiller energy consumptions were similar to those of the normal case (Figure 11). Additionally, the energy consumption in Cases A-1 and A-2 varied based on the fault frequency and offset, as observed in the evaluation of the indoor thermal comfort. The fixed-offset cases (Cases B-1 and B-2) experienced faults with negative offsets in the SCWT sensor, resulting in reductions of approximately 1.3% and 0.8% in chiller energy consumption, respectively, compared with that of the normal case. This was because the compressor workload was reduced as the SCWT did not reach the set value (Figure 11a). To compensate for this, the circulation pump energy consumption increased by approximately 19.2% and 7.1% (Figure 11b), and the fan energy consumption increased by 11.8% and 0.9% for Cases B-1 and B-2, respectively (Figure 11c). However, Cases B-3 and B-4, with positive offsets in the sensor faults, resulted in increases of approximately 1.3% and 2.1% in chiller energy consumption, respectively, owing to the increased compressor workload (Figure 11a). The circulation pump energy consumption decreased by approximately 5.7% and 14.3% for Cases B-3 and B-4, respectively, as the supply chilled water flow rate decreased (Figure 11b). This was because the SCWT value was lower than the set value. In this case, the chilled water still supplied the heat required for air conditioning; thus, the fan energy consumption remained the same as that in the normal case (Figure 11c). Case C involved random sensor fault offsets, which resulted in increases of approximately 0.6%, 2.9%, and 1.5% in the chiller, circulation pump, and fan energy consumptions, respectively, compared with those of the normal case (Figure 11). Among the drift offset cases, the negative sensor fault offset worsened over time in Case D-1, resulting in a decrease of approximately 10.5% in the chiller energy consumption compared with that of the normal case (Figure 11a). To compensate for this, the circulation pump and fan energy consumptions increased by approximately 23.6% (Figure 11b) and 42.6% (Figure 11c), respectively. Case D-2 had a positive sensor fault offset, which led to an increase of approximately 1.8% in the chiller energy consumption compared with that of the normal case (Figure 11a). The circulation pump energy consumption decreased by approximately 17.1% owing to the lower SCWT (Figure 11b). However, the fan energy consumption remained the same as that in the normal case (Figure 11c).

The evaluation results demonstrated that the impact of sensor faults on energy consumption varied depending on the offset value and frequency of fault occurrence in the cases of point and random offsets. In the cases of fixed and drift offsets, faults with a positive offset led to an increase in the chiller energy consumption and a decrease in circulation pump consumption. Conversely, faults with a negative offset resulted in a decrease in circulation pump and fan energy consumptions and an increase in the chiller energy consumption (Table 7).

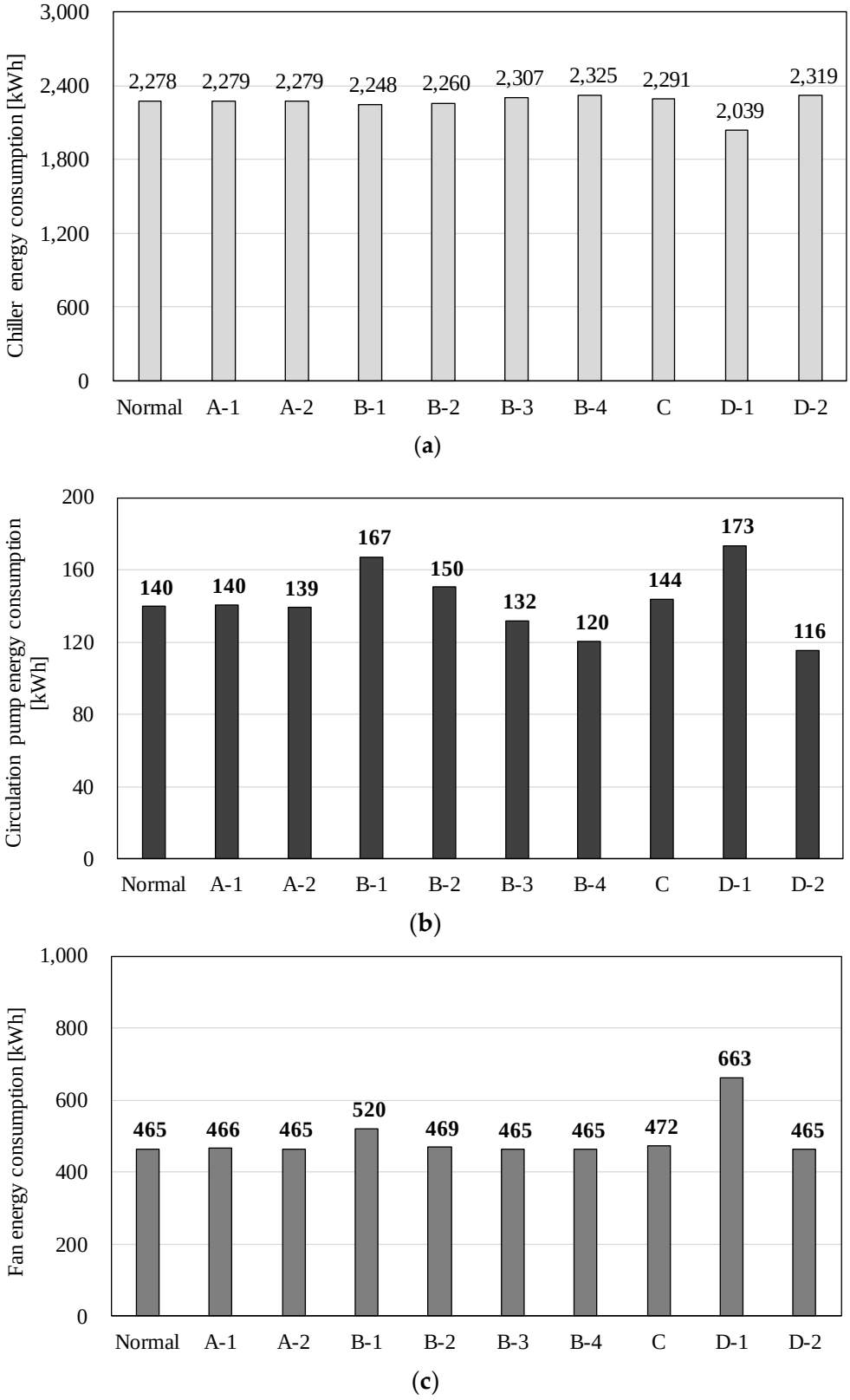

Figure 11. Monthly energy consumptions for various fault types: (**a**) chiller energy consumption; (**b**) circulation pump energy consumption; and (**c**) fan energy consumption.

Table 7. Effects on energy consumption for various fault types and offsets.

Offset Types	Equipment	Negative Offset	Positive Offset
Point	Chiller Circulation pump Fan	Depended on offset value and frequency	
Fixed	Chiller Circulation pump Fan	Decrease Increase Increase	Increase Decrease -
Random	Chiller Circulation pump Fan	Depended on offset value and frequency	
Drift	Chiller Circulation pump Fan	Decrease Increase Increase	Increase Decrease -

The results of evaluating unmet hours and energy consumption indicate the necessity of periodic sensor fault detection using the virtual sensor developed in this study to prevent worsening indoor thermal comfort and increased energy consumption.

6. Conclusions

The objective of this study was to develop a virtual sensor based on an LSTM-autoencoder to detect faults in a SCWT sensor that negatively impact HVAC systems. To achieve this, a simulation model (building, HVAC system, and SCWT sensor faults) was developed using EnergyPlus, and a virtual sensor was developed to detect faults in the SCWT sensor. Subsequently, a case study was conducted to evaluate the fault-detection performance and correction effects of the virtual sensor. The conclusions of this study are as follows.

- The evaluation of the fault-detection performance of the virtual sensor showed excellent results for various fault types. The virtual sensor detected all faults for the transient fault types (Cases A-1 and A-2), with an F-1 score of 1.000. The virtual sensor detected the majority of faults for the continuously fixed fault types (Cases B-1 to B-4), with F-1 scores ranging from 0.9965 to 0.9997. However, the virtual sensor occasionally failed to detect faults with subtle offsets for continuous random offset faults (Case C) and faults with offsets that gradually increased or decreased over time (Cases D-1 and D-2), resulting in F-1 scores ranging from 0.9350 to 0.9846.
- The evaluation of indoor thermal comfort following fault resolution revealed that the impact of sensor faults on indoor thermal comfort in types with transient and random offsets varied depending on the occurrence frequency and offset of the sensor faults. In the case of faults with continuously fixed offsets and offsets worsening over time, the indoor set-point temperature unmet hours increased by up to 425% for negative fault offsets. Consequently, indoor thermal comfort was adversely affected.
- The evaluation of energy consumption following fault resolution revealed that the impact of sensor faults on energy consumption in types with transient faults and random offsets varied depending on the occurrence frequency and offset of the sensor faults. In the case of faults with continuously fixed offsets and those with offsets worsening over time, the chiller energy consumption decreased for faults with negative offset values, whereas the circulation pump and fan energy consumption increased. Conversely, for faults with positive offset values, the chiller energy consumption increased, whereas the circulation pump energy consumption decreased.

The results of this study suggest the necessity of periodic sensor fault detection using a virtual sensor to simultaneously achieve indoor thermal comfort satisfaction and prevent excessive energy consumption. However, the virtual sensor developed in this study was trained based on simulation data. Validation with actual building data will be

required in the future to consider the applicability of the virtual sensor to an actual building. Additionally, comparisons and analyses with state-of-the-art models are also required as sensor fault-detection models continue to be developed.

Author Contributions: All authors contributed equally to this study. Conceptualization, S.J. and S.L.D.; methodology, S.J. and S.L.D.; formal analysis, S.J., A.J. and S.L.D.; data curation, S.J., A.J. and S.L.D.; writing—original draft preparation, S.J. and S.L.D.; writing—review and editing, D.L., S.K., M.S. and S.L.D.; visualization, S.J., A.J., D.L., S.K., M.S. and S.L.D.; supervision, S.L.D. All authors have read and agreed to the published version of the manuscript.

Funding: This work was supported by the National Research Foundation of Korea (NRF) grant funded by the Korea government (MSIT). (No. 2021R1C1C1010231).

Institutional Review Board Statement: Not applicable.

Informed Consent Statement: Not applicable.

Data Availability Statement: Data are contained within the article.

Conflicts of Interest: The authors declare no conflict of interest.

References

1. MOTIE. *Energy Consumption Survey*; South Korea Ministry of Trade, Industry and Energy (MOTIE): Sejong City, Republic of Korea, 2020.
2. KEEI. *Monthly Energy Statistics*; Korea Energy Economics Institute (KEEI): Ulsan, Republic of Korea, 2023.
3. Jin, S.; Kim, D.; Do, S.L. Evaluation of Influence on Cooling System by Faulty Temperature Sensor of Supply Chilled Water. *J. Archit. Inst. Korea Struct. Constr.* **2023**, *39*, 207–213.
4. Katipamula, S.; Brambley, M.R. Review Article: Methods for Fault Detection, Diagnostics, and Prognostics for Building Systems-A Review, Part I. *HVAC&R Res.* **2005**, *11*, 3–25. [CrossRef]
5. Schein, J.; Bushby, S. *A Simulation Study of a Hierarchical, Rule-Based Method for System-Level Fault Detection and Diagnostics in HVAC Systems*; National Bureau of Standards: Gaithersburg, MD, USA, 2005. [CrossRef]
6. Yang, H.; Cho, S.; Tae, C.S.; Zaheeruddin, M. Sequential Rule Based Algorithms for Temperature Sensor Fault Detection in Air Handling Unit. *Energy Convers. Manag.* **2008**, *49*, 2291–2306. [CrossRef]
7. Schein, J.; Bushby, S.T.; Castro, N.S.; House, J.M. A Rule-Based Fault Detection Method for Air Handling Unit. *Energy Build.* **2006**, *38*, 1485–1492. [CrossRef]
8. Guo, Y.; Wang, J.; Chen, H.; Li, G.; Huang, R.; Yuan, Y.; Ahmad, T.; Sun, S. An Expect Rule-Based Fault Diagnosis Strategy for Variable Refrigerant Flow Air Conditioning Systems. *Appl. Energy* **2019**, *149*, 1223–1235. [CrossRef]
9. Wang, S.; Chen, Y. Sensor Validation and Reconstruction for Building Central Chilling Systems Based on Principal Component Analysis. *Energy Convers. Manag.* **2004**, *45*, 673–695. [CrossRef]
10. Wang, S.; Zhou, Q.; Xiao, F. A System-level Fault Detection and Diagnosis Strategy for HVAC Systems Involving Sensor Fault. *Energy Build.* **2010**, *42*, 477–490. [CrossRef]
11. Yan, Y.; Cai, J.; Tang, Y.; Yu, Y. A Decentralized Boltzmann-machine-based Fault Diagnosis Method for Sensors of Air Handling Units in HVACs. *J. Build. Eng.* **2022**, *50*, 104130. [CrossRef]
12. Lee, W.Y.; House, J.M.; Kyoung, N.H. Subsystem Level Fault Diagnosis of a Building's Air-handling Unit Using General Regression Neural Networks. *Appl. Energy* **2004**, *77*, 153–170. [CrossRef]
13. Du, Z.; Fan, B.; Chi, J.; Jin, X. Sensor Fault Detection and Its Efficiency Analysis in Air Handling Unit Using the Combined Neural Networks. *Energy Build.* **2014**, *72*, 157–166. [CrossRef]
14. DOE. *Energyplus*, Version 9.3; Department of Energy (DOE): Washington, DC, USA, 2020.
15. Bengio, Y.; Simard, P.; Frasconi, P. Learning Long-term dependencies with gradient descent is difficult. *IEEE Trans. Neural Networks* **1994**, *5*, 157–166. [CrossRef] [PubMed]
16. Hochreiter, S.; Schmidhuber, J. Long Short-term Memory. *Neural Comput.* **1997**, *9*, 1735–1780. [CrossRef] [PubMed]
17. Sendra-Arranz, R.; Gutiérrez, A. A Long Short-term Memory Artificial Neural Network to Predict Daily HVAC Consumption in Buildings. *Energy Build.* **2020**, *216*, 109952. [CrossRef]
18. Zhu, H.; Yang, W.; Li, S.; Pang, A. An Effective Fault Detection Method for HVAC Systems Using the LSTM-SVDD Algorithm. *Buildings* **2022**, *12*, 246. [CrossRef]
19. Liu, X.; Ren, M.; Yang, Z.; Yan, G.; Guo, Y.; Cheng, L.; Wu, C. A Multi-step Predictive Deep Reinforcement Learning Algorithm for HVAC Control Systems in Smart Buildings. *Energy* **2022**, *259*, 124857. [CrossRef]
20. Cong, Y.; Hou, L.; Wu, Y.; Ma, Y. Development of a Coupled EnergyPlus-MATLAB Simulation Based on LSTM for Predictive Control of HVAC System. *Math. Probl. Eng.* **2022**, *2022*, 5912967. [CrossRef]
21. DOE. *Commercial Prototype Building Models*; Department of Energy (DOE): Washington, DC, USA, 2019.

22. ASHRAE. *International Weather Files for Energy Calculation 2.0*; American Society of Heating, Refrigerating and Air-conditioning Engineers (ASHRAE): Atlanta, GA, USA, 2017.
23. Varun, C.; Arindam, B.; Vipin, K. Anomaly detection: A Survey. *ACM Comput. Surv.* **2009**, *41*, 15.